Role of Si on the surface damage mechanism of RB-SiC/Si under mechanical loading

Quanli Zhang[1*], Zhen Zhang[1], Honghua Su[1], Qingliang Zhao[2], and Suet To[3]

[1] College of Mechanical and Electrical Engineering, Nanjing University of Aeronautics and Astronautics, Nanjing 210016, China

[2] Centre for Precision Engineering, School of Mechatronics Engineering, Harbin Institute of Technology, Harbin, 150001, China

[3] State Key Laboratory of Ultra-precision Machining Technology, The Hong Kong Polytechnic University, Hong Kong

*Corresponding Author / E-mail: zhangql606@163.com, TEL: +86-025-84892901, FAX: +86-025-84895857

Abstract

Indentation test (Nano-indentation and Vickers-indentation), diamond scratching and high spindle speed grinding (HSSG) are conducted to investigate the role of silicon (Si) on the surface damage behavior of reaction bonded SiC/Si composites (RB-SiC/Si). Even though the addition of Si contributes to densifying the bulk materials and improving the toughness, the indentation and diamond scratching results firstly indicate that the cracks initiate at the SiC/Si interfaces due to the non-uniform deformation caused by the existence of Si, and the phase transformation of Si also leads to the pop-out effect during the nano-indentation and the diamond scratching test. The ground surface of RB-SiC/Si is characterized by scratching grooves and brittle fracture, indicating the ductile material removal mode and brittle material removal mode for RB-SiC/Si, respectively, and the surface reliefs form on the ground surface due to the different hardness between Si and SiC phases. Moreover, the phase transformation of Si contributes to the easy fracture of phase boundaries under the mechanical loading, and the accompanied volume change also results in the dislodgement of hard particles and the generation of surface burs on the ground surface.

Keywords: RB-SiC/Si; Grain boundaries; Phase transformation; Fracture; Grinding

Nomenclature used in this article

B= brittleness of the material

E = elastic modulus

H= vickers hardness

K_C =fracture toughness

ρ=material density

a_e= depth of cut

F=feed rate

P= the indentation load

L= the crack length by indentation

a=the diagonal length of the imprint

C=L+a

1. Introduction

Reaction bonded silicon carbides (RB-SiC) are widely applied in the nuclear field, the optical industry and the electronic industry for the excellent mechanical properties at the high temperature and in the harsh environments, which contribute to the longer service life of the devices and environmental manufacturing (Ref 1-5). Actually, the melted Si can fill the pores among the SiC grains during the sintering process through the formation of the chemical bonds between Si and SiC (Ref 6, 7), but the incomplete reaction of Si resulted in a certain remaining amount of free silicon (Si) in the bulk material (Ref 7-9).

As far as the great hardness and brittleness of SiC is concerned, the machinability and the high precision manufacturing technologies of SiC materials have been widely investigated. First of all, to improve the surface integrity of the machined SiC parts, the ductile material removal should be achieved. A critical indentation load for the SiC materials can be approximately determined by the indentation method, and the main damage mechanism for both single crystalline SiC and poly-crystalline SiC is cleavage fracture when the load is greater than the threshold (Ref 10,11). For RB-SiC/Si, the existence of the phase boundaries between Si and SiC led to the heterogeneity of the microstructure, and the bulk material dislodgement resulting from the crack initiation and propagation during grinding led to the high cost for the production process (Ref 12). Agarwal (Ref 13,14) reported that the efficiency of the grinding process can be improved by the brittle material removal and an improvement of the surface quality was achieved by optimizing the machining parameters (Ref 15). For the simplification and cost-effectiveness, diamond scratching has been undertaken to investigate the material removal mechanism during grinding and the correlation between the surface roughness and the subsurface damage (Ref 16-18). It was found that the high pressure phase transformation (HPPT) of Si can be induced under the mechanical loading, and the accompanied volume change prompted the surface fracture which led to the dropping critical depth of cut than the calculated result (Ref 19-21). More specifically, the accompanied 22% volume decrease caused by the phase transformation from Si-I to Si-II results in the decreasing slope of the load-displacement curve at this point, while the

volume expansion occurred during the transformation from β-Sn structure (Si-II) to R8 structure (Si-XII) which further transformed to Si-III. Both the volume decrease and increase led to the generation of the abnormal load-displacement curves (elbow or pop-out). Therefore, the existence of Si in the bulk materials has great influence on the surface damage mechanics of RB-SiC/Si under the mechanical loading. Nevertheless, the impact of Si on the nanometric surface characteristics of RB-SiC/Si under grinding is still lack of direct and comprehensive investigation, and the damage mechanics under the varied mechanical loading deserve much more attention.

In this study, the quasi-static mechanic behavior of RB-SiC/Si is firstly explored by nanoindentation and Vickers hardness indentation test, focusing on the effects of Si. To elucidate the impact of Si, the Vickers hardness indentation tests of single crystal SiC and Si were also performed for comparison. Then, the diamond scratching of RB-SiC/Si is undertaken to illustrate the material removal mechanism under the dynamic loading. Finally, the impact of Si on the nanometric surface characteristics of RB-SiC/Si composites during the high spindle speed grinding (HSSG) is explored.

2. Materials and experiments

The workpiece material is commercially available RB-SiC/Si composite (Goodfellow Cambridge Ltd., UK), in which about 10 wt.% free silicon remains and the diameter of the SiC particles is about 10 μm, and single crystalline Si and 6H-SiC (Xiamen Powerway Advanced Material Co., Ltd., China) are also used for the comparison experiments. Table 1 lists the detailed mechanical properties of RB-SiC/Si. Before the indentation and the scratching tests, the workpiece material was firstly polished with the diamond paste by hand and the surface roughness (Ra) after polishing was about 10 nm.

Table 1 Detail mechanical properties of the RB-SiC/Si material

RB-SiC/Si	~10 wt.% Si
Elastic modulus E (GPa)	410
Vickers hardness H (kgf mm^{-2})	2500
Fracture toughness K_{IC} (MPa m$^{1/2}$)	3
Compressive strength (MPa)	2000
Density ρ (g/cm^3)	3.1

Nanoindentation test (Nano-Indenter® XP system, MTS) was undertaken to characterize the varied mechanical properties of RB-SiC/Si at different points. The tip used for the nanoindentation test was Berkovich tip and the test was performed in the continuous stiffness measurement (CSM) mode. Five repeated indentations at each parameter were conducted to make the results more reliable. To illustrate the damage mechanics of RB-SiC/Si at higher loads, the Vickers indentation (MicroWiZhard) at 0.2 kg was performed for three repeated times, with the loading/unloading time of 5 s and the holding time of 10 s. The indentation tests on the monocrystalline SiC and monocrystalline Si were also performed for comparison. The diamond scratching test was then performed on a precision grinding machine (MUGK7120X5, Hangzhou Machine Tool Group Co., Ltd., China), with the diamond grit fixed to a steel disc and the diameter of the sharp point was around 230 mm. The scratching setup is shown in Fig. 1. High spindle speed grinding (HSSG) was conducted on a three-axes ultra-precision grinding machine (450UPL, Moore Nanotech. USA). The scratching parameters and the grinding parameters are listed in Table 2 and Table 3, respectively. Illustration of the grinding setup can be found in our previous study (Ref 22).

Table 2 Detail parameters of the scratching test

Machine	MUGK7120X5
Grit shape	Face to face apex angle 120°
Scratching diameter	230 mm
Rotation speed	50 RPM
Feed rate	1000 mm/min

Table 3 Detail parameters of the high spindle speed grinding

Wheel (20 mm in diameter)	1500#G0787B195
Wheel rotation speed (rpm)	20,000
Workpiece rotation speed (rpm)	120
Depth of cut (μm)	0.5
Feed rate (mm/min)	0.5
Coolant	CLAIRSOL 350
Size of the workpiece	16×16×5 mm

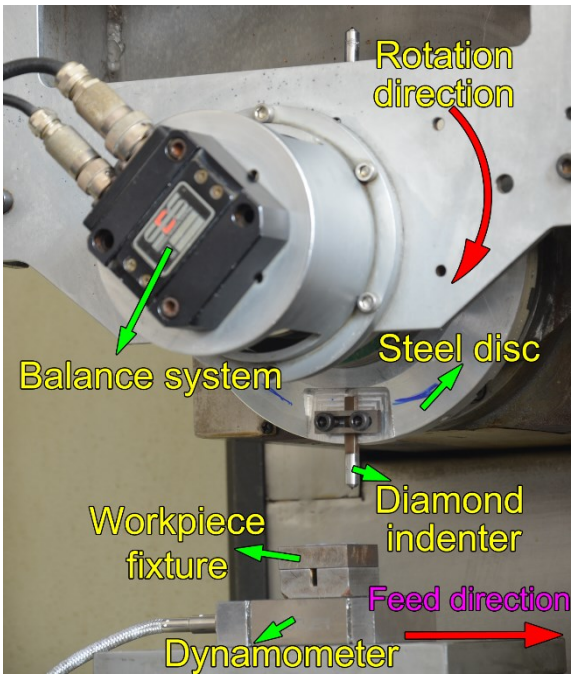

Fig. 1 Illustration of the setup for the diamond scratching

The surface morphology of the polished RB-SiC/Si surface was checked by an optical microscope (Olympus BX60) and a white light interferometer (WLI, ZYGO Lamda Nexview). The indentation imprints and the scratching grooves were characterized by a scanning electron microscope (SEM, Hitachi TM3000) and the white light interferometer, and focused ion beam (FIB, JEOL Model JIB-4501) was utilized to examine the scratched surface. The ground surface of RB-SiC/Si was examined by a scanning electron microscope (SEM, JEOL Model JSM-6490), an atomic force microscope (AFM, Park's XE-70) and the white light interferometer to identify the surface characteristics. In addition, the machined surface of RB-SiC/Si was characterized by Raman spectroscopy (JYHR800, Horiba) to study the phase transformation of Si, where the laser wavelength is 458 nm and the spot size is around 1 μm.

3. Results and discussion

3.1 Damage mechanism of RB-SiC/Si under indentation

Fig. 2 shows the typical load-displacement curves of the nanoindentation test for RB-SiC/Si at different loading/unloading conditions. When the maximum load was 5 mN, no obvious plastic deformation of SiC phase appeared, as shown in Fig. 2(a). The further increase of the maximum loads to 25 mN and 50 mN result in higher residual

deformation, but the curvatures do not change evidently at the loading and unloading stage. On the contrary, an 'elbow' begins to occur at the unloading stage for Si even with the maximum load of 5 mN, which becomes more obvious at the maximum load of 25 mN, as shown in Fig. 2(b). Moreover, it can be found that the 'pop-out' effect appears during the unloading stage for the Si phase as the maximum load reaches 50 mN. The specific phenomenon indicates that the phase transformation of Si was induced and the volume change accompanied during the fast unloading stage promoted the appearance of the surface fracture (Ref 21, 23-25).

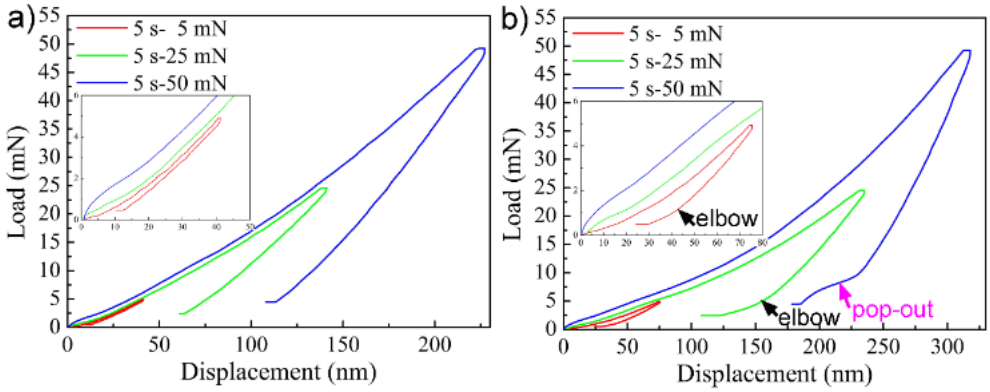

Fig. 2 Load-displacement curves of the SiC and the Si phases in RB-SiC/Si at a loading/unloading time of 5 s and with the varied maximum loads: (a) for SiC phases, (b) for Si phases

To get a further insight into the impact of the phase boundaries on the surface damage mechanism, the nannoindentation test was also conducted on the polished RB-SiC/Si surface at the max load of 100 mN with the loading/unloading time of 20 s. The surface morphologies and the load-displacement curves of three typical indentation imprints at different points are shown in Fig. 3. The positions are numbered in the optical image, as shown in Fig. 3(a). Position 1 is the phase boundary of SiC and Si, while position 2 is nearly on the SiC phase. Indentation test at position 3 is totally conducted on the SiC phase. It can be easily found that obvious surface fracture was induced at the phase boundaries of SiC and Si at *Position 1*. According to the previous studies (Ref 26-29), the ratio of the hardness to the fracture toughness (H/K_{IC}) can be seen as the index of the brittleness of the material, which can be calculated by Equ.(1). Based on the results of the nanoindentation text, the brittleness (B) of the different phases (SiC and Si),

as well as the phase boundaries can be ordered as: $B_{Phase\ boundaries}>B_{SiC}>B_{Si}$. The higher brittleness, the easier occurrence of the surface fracture (Ref 26).

$$B = \frac{H \cdot E}{K_C^2} \tag{1}$$

In addition, it can be easily seen that the phase boundary between the Si and the SiC phase results in the non-coordinated deformation during the loading and unloading stages. As shown in Fig. 3(b), the surface fracture also results in the abnormal curve in the loading stage. Besides, the degree of the deformation for the different indentation points also differed under the same loading conditions, which was attributed to the varied hardness of SiC and Si, as well as the random phase distribution. The non-uniform deformation of Si and SiC resulted in the phase boundaries fracture easier. On the one hand, the phase transformation induced volume change of Si under the high pressure near the indenter contributed to the boundary damage, as has been reported in the previous studies (Ref 19, 20). On the other hand, the surface damage is dependent on the percentage of the area of the Si phase in the imprint, where the surface fracture of the indented position appeared if the imprint was mainly on the Si phase between the two neighboring SiC grains. It has been reported that the strengthening effects of GNDS (geometrically necessary dislocations) is limited as the deformation goes beyond a single grain (Ref 30), so the surrounding phase effects should be taken into consideration to explain the result. When the nano-indentation test was undertaken on the SiC phases, the surrounding Si phases contributed to the plastic deformation for its lower hardness compared with the SiC phases. On the contrary, the SiC phases around Si worked as rigid substrates when the imprints were performed on the Si phases, so the volume change of Si caused by phase transformation is limited, which promotes the surface fracture of the phase boundaries.

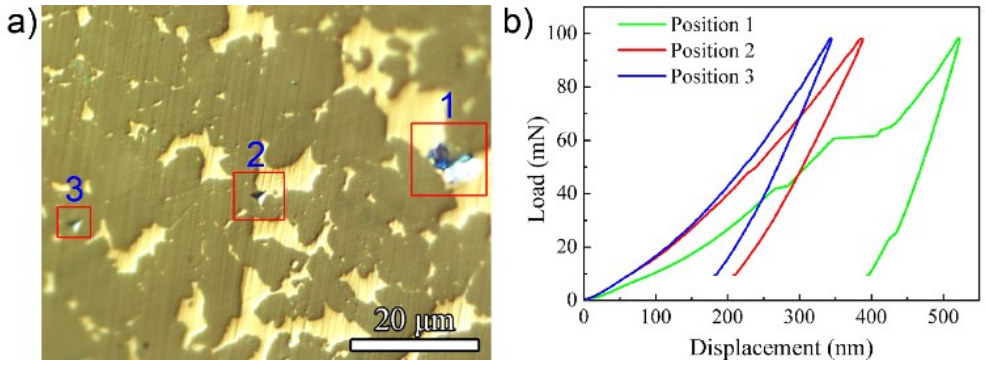

Fig. 3 (a) The surface morphologies of three typical imprints conducted at the varied points, (b) the corresponding load-displacement curves

Fig. 4 shows the BSEM images and the surface topographies of the Vickers-hardness indentation imprints of monocrystalline 6H-SiC, monocrystalline Si and RB-SiC/Si at the maximum load of 0.2 kg, respectively. As shown in Fig. 4(a) and Fig. 4(b), the radial cracks on both of the single crystalline Si and 6H-SiC are obviously induced under the Vickers indentation, and the indented depth and the generated plastic deformation on Si are greater than 6H-SiC due to the different hardness. Moreover, from the 3D surface topographies of the imprints, it can be found that the single crystalline Si surface is obviously extruded and swelled near the imprints. As shown in Fig. 4(c), obvious radial and lateral cracks are also induced around the four edges on the polished RB-SiC/Si at the same load, and the propagation of the radial cracks is dependent on the relative direction between the crack tip and the phase boundaries. Specifically, the generated cracks are more like to initiate and propogate if the phase boundary is nearly parallel to the generated radial cracks. However, when the angle between the phase boundary and the radial crack is in the range of 45-90°, the lengths of the radial cracks decrease compared with the monocrystalline Si and 6H-SiC. For a multi-phase composite, the formation and propagation of the radial cracks can be classified into transgranular cracks, intergranular fracture, crack deflection, crack bridging and crack pinning. For RB-SiC/Si, the grain boundaries between the SiC and the Si phases result in an increase of the propagation path, which consume more energy. In addition, the appearance of the transgranular cracks, crack deflection and crack pinning need to overcome the residual stress and increase the energy dissipation. Therefore, the lengths of the radial cracks for the SiC and the Si phases in RB-SiC/Si dropped, compared with that of the

monocrystalline SiC and Si. This is a good indication that the free Si in the bulk RB-SiC/Si could improve the toughness to some degree according to Eqs. (2) and (3) (Ref 2, 31).

$$K_c = 0.0098\left(\frac{E}{H}\right)^{3/2} \cdot P \cdot C^{-3/2}, \quad L/a > 2.5 \tag{2}$$

$$K_c = 0.015\left(\frac{L}{a}\right)^{-1/2} \cdot \left(\frac{E}{H}\right)^{3/2} \cdot P \cdot C^{-3/2}, \quad L/a < 2.5 \tag{3}$$

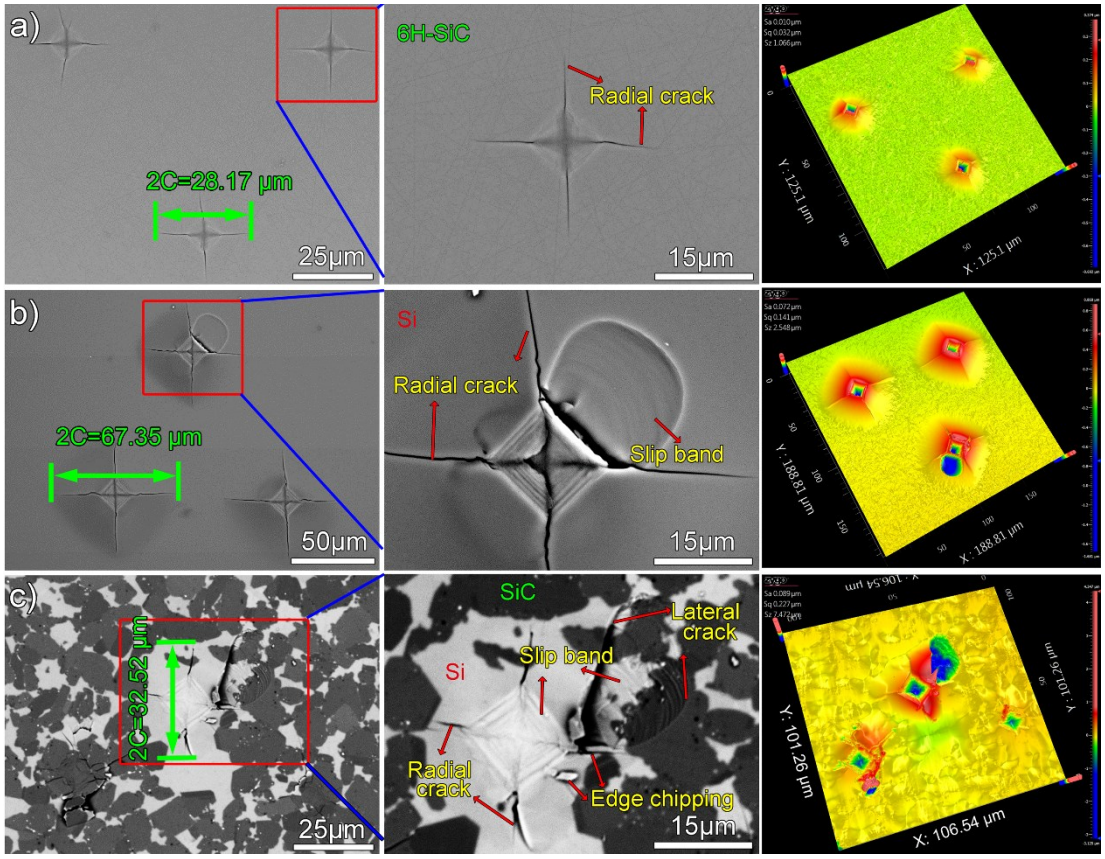

Fig. 4 BSEM images and surface topographies of the Vickers-hardness indentation imprints at the maximum load of 0.2 kg: (a) monocrystalline 6H-SiC, (b) single crystalline Si, (c) RB-SiC/Si

However, as far as the size of the indentation imprint is greater than the grain size of the SiC phase, the higher brittleness of the phase boundaries between the Si and the SiC phases results in the surface fracture. Meanwhile, the surface integrity of the RB-SiC/Si composites obviously dropped as the fracture and chipping occurred at the phase boundaries of SiC and Si. Interestingly, the formation and propagation of the lateral

cracks and the slip bands resulted in the generation of a cave and some ripples for the monocrystalline Si and the Si phase in RB-SiC/Si. Under the indentation load, the plastic deformation occurs firstly and the radial cracks are then induced at the points of the sharp edges, followed by the formation of the lateral cracks as the deformation reaches the fracture strength (Ref 29, 32, 33). For RB-SiC/Si, the edge chipping appeared during the indentation test, and the first appearance of the cracks at the phase boundaries indicated that the remnant Si in the bulk RB-SiC/Si material led to the weakened interfaces, which can be attributed to the stress concentration resulted from the non-uniform plastic deformation of SiC and Si at the phase boundaries.

3.2 Damage mechanism of RB-SiC/Si under diamond scratching

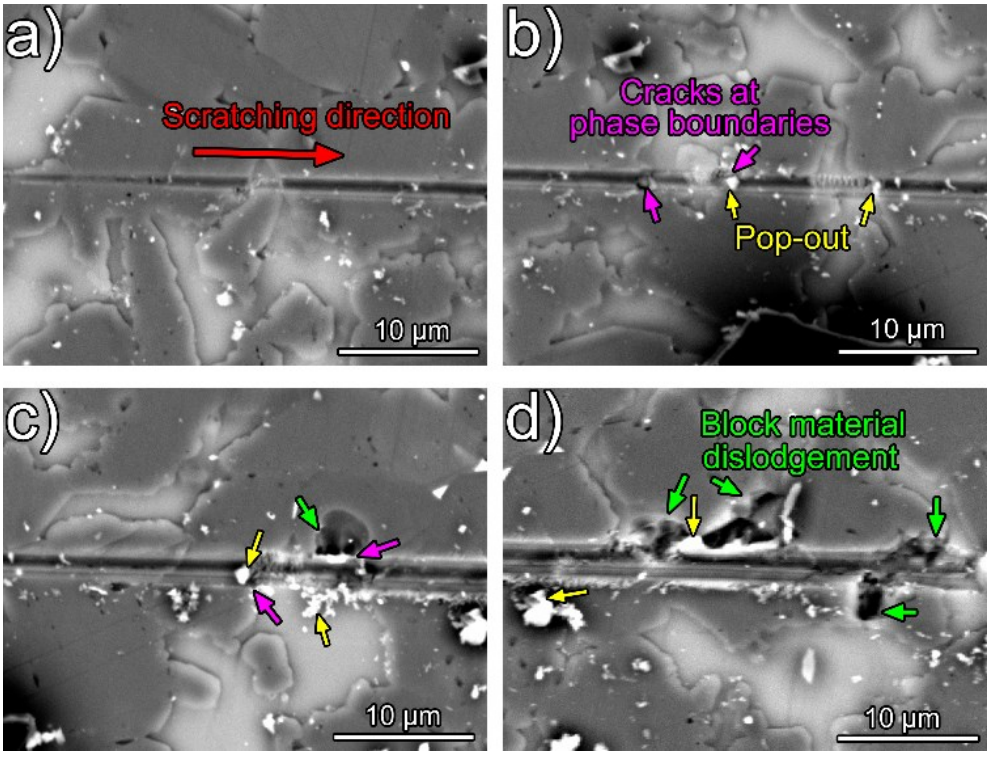

Fig. 5 BSEM images of the diamond scratching grooves at different positions with increasing cutting depth

From the surface morphology of the diamond scratching groove, as shown in Fig. 5(a), it can be clearly seen that the ductile scratching grooves formed at the beginning of the scratch and no obvious chips remained on the workpiece surface, but some discontinuous bulges, as well as some micro-ridges, appeared on the Si phases, as shown in Fig. 5(b). With the increase of the cutting depth, obvious chips were generated and left

on the workpiece surface. It is interesting to find that the cracks firstly appeared at the phase boundaries of SiC/Si, although the material removal modes for both Si and SiC phases are ductile. As the cutting depth increased continuously, lateral cracks were induced at the sides of the grooves, and their propagation prompted the bulk material dislodgement. Therefore, the scratching groove was characterized by the bulk material fracture and the random distributed block chips near the groove, as shown in Fig. 5(c) and Fig. 5(d).

To get a further insight into the subsurface damage mechanism of RB-SiC/Si under the dynamic loading condition, FIB section of the scratched groove was undertaken and the subsurface morphology is shown in Fig. 6. The formed cracks between the SiC and Si phase propagated along the boundary to a certain depth that was about in the size of a SiC grain diameter in the selected position, and a layer of serious deformed substance was induced under the dynamic loading of the diamond indenter.

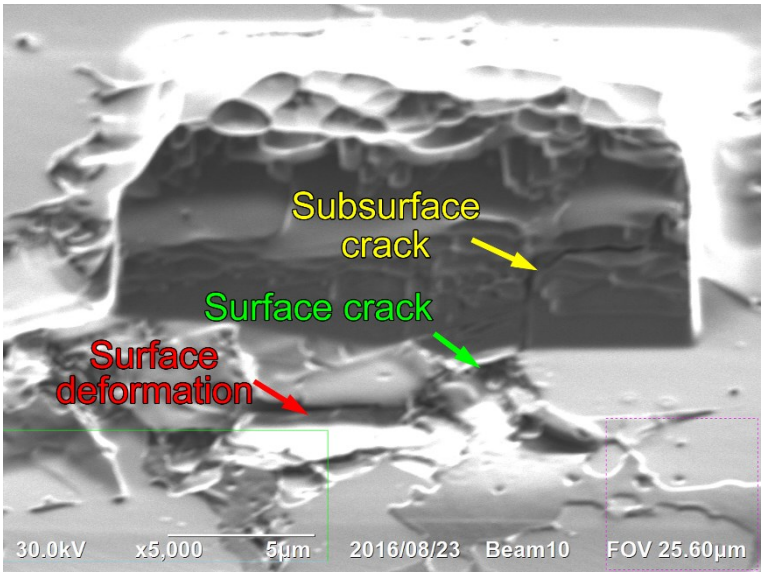

Fig. 6 FIB section of the scratching groove on RB-SiC/Si

In addition, the phase transformation induced volume change also affect the fracture depth (Ref 20), which is indicated by the yellow arrows in Fig. 5. The surface topography of the scratched surface is shown in Fig. 7. It can be readily seen that the plastic deformation was induced at the initial stage of the scratching on both of the SiC and the Si phases, as shown in position A in Fig. 7. With the increase of the cutting depth, protrusion appeared at the phase boundary due to the phase transformation

(Position B and C in Fig. 7). The different hardness between SiC and Si also contributes to the formation of pits as the diamond grit went through from SiC to Si, which even appeared at the initial scratching stage.

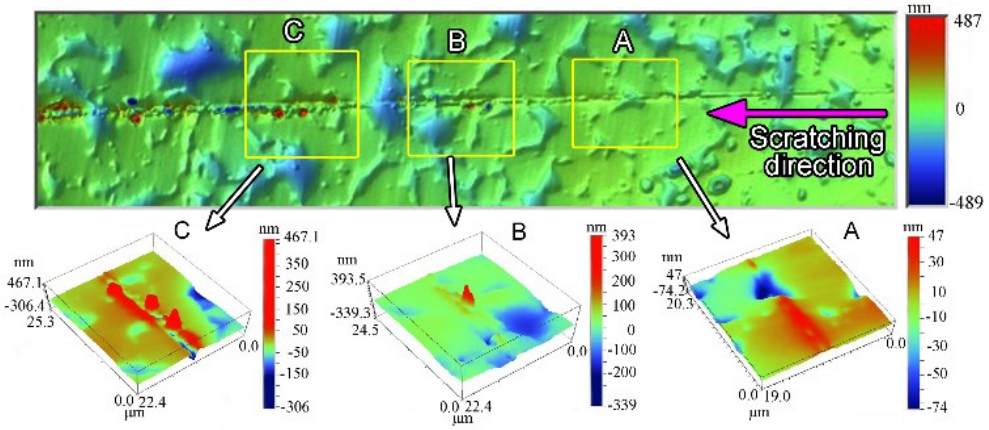

Fig. 7 Surface topography of the scratched groove on RB-SiC/Si with increasing cutting depth

3.3 Damage mechanism of RB-SiC/Si under grinding

The surface morphology and surface topography of the ground RB-SiC/Si carbides are shown in Fig. 8. It can be found that the machined surface of RB-SiC/Si is covered by the randomly distributed micro-pits at the phase boundaries and the plastic scratching grooves, as shown in Fig. 8(a) and Fig. 8(b). The surface quality was aggravated by the block shedding and tearing of the workpiece materials, leaving deeper pits on the machined surface. From the indentation results, it can be said that the existing phase boundaries between SiC and Si promoted the edge chipping and the increased fracture degree. In addition, it is interesting to find that the phase boundaries with a small angle to the grinding direction (nearly in parallel direction) tend to be broken under grinding, while those perpendicular to the moving direction of the diamond grits are of good integrity, as shown in Fig. 8(a) and Fig. 8(b). This corresponds with the indentation results, as shown in Fig. 4(c).

Moreover, it can be found from the 3D surface topography of RB-SiC/Si that some projections formed and distributed randomly on the machined surface, as shown in Fig. 8(c). The formation of the reliefs on the machined surface appeared as the residual height of the SiC phase is obvious higher than the Si phase for their different hardness. The lower hardness of Si resulted in the greater penetration depth of the diamond grits

and thus greater material removal volume. For comparison, high spindle speed grinding of the single crystalline Si and 6H-SiC was also conducted under the same condition, and the typical surface topographies of the ground surface at the same radial position of the machined RB-SiC/Si, the single crystalline Si and 6H-SIC surface are shown in Fig. 8 (d), (e) and (f), respectively. It can be seen that the accompanied volume change of the Si phase transformation resulted in the material dislodgement which is of the similar surface characteristics with that of RB-SiC/Si, and the ground surfaces are both much rougher than 6H-SiC, indicated by the typical surface roughness parameters (Ra, Rq, Rt).

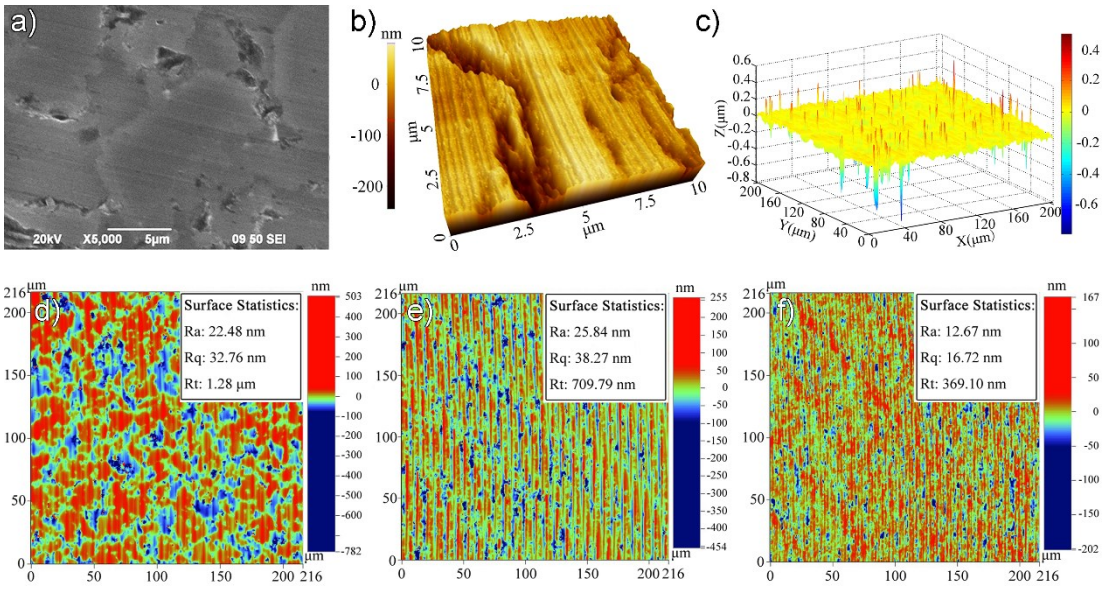

Fig. 8 (a) SEM image of RB-SiC/Si after grinding, (b) 3D surface topography of RB-SiC/Si after grinding measured by AFM, (c) 3D surface topography of RB-SiC/Si after grinding measured by WLI viewed from 45°, (d), (e) and (f) 3D surface topographies of RB-SiC/Si, single crystalline Si and 6H-SiC after grinding measured by WLI viewed from 90°

The Raman spectra of the Si phase of the ground RB-SiC/Si surface showed that the phase transformation of Si was induced by the dynamic pressure of the diamond grits, which is indicated by the appearance of the broad peaks at around 154 cm^{-1} and 520 cm^{-1}, which corresponds to the crystalline Si-III and Si-I phase, respectively (Ref 23, 34), as shown in Fig. 9. The volume change caused by the phase transformation promoted the fracture of the phase boundaries between SiC and Si, so the critical cutting

depth for the ductile to brittle transformation became much smaller than the theoretical value (Ref 35, 36). In addition, the volume change accounts for the formation of the burs on the ground surface shown in Fig. 8(c).

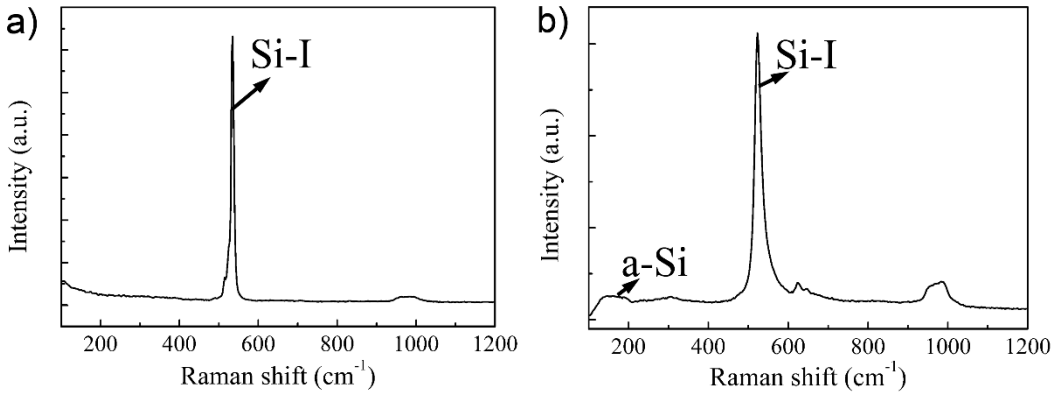

Fig. 9 Raman spectra of the Si phase of RB-SiC/Si before and after the grinding process: (a) before grinding, (b) after grinding

4. Conclusions

In the present work, the surface damage mechanism of RB-SiC/Si under the varied mechanical loading at room temperature, including the indentation, the diamond scratching and the high speed spindle grinding (HSSG), is systematically investigated. The role of the Si phases on the nanometric surface characteristics is discussed, which can establish a good foundation for the ultra-precision machining of RB-SiC/Si. Based on the above experimental results and discussion, the following conclusions can be drawn:

(1) Even though the existence of the Si phases contributes to densifying the bulk material and improving the toughness of RB-SiC/Si, the phase boundaries become the fragile position in the bulk materials for RB-SiC/Si, where cracks and edge chipping were easily induced during the indentation and the diamond scratching;

(2) Nano-indentation results show that the plastic deformation for Si and SiC differed under the same loading/unloading condition, and the existence of the Si phases in the bulk RB-SiC/Si results in the obvious disparity of the measured elastic modulus and hardness at different positions, which contributes to the preferential formation of the cracks at the phase boundaries during the diamond scratching. The different material removal rate of Si and SiC due to the varied hardness leads to the occurrence of the

surface reliefs on the ground surface by high spindle speed grinding (HSSG);

(3) The phase transformation of Si occurs under the mechanical loading, indicated by the formation of 'elbow' and 'pop-out' during the nano-indentation and the decreasing peak intensity of Raman spectra at 154 cm^{-1} and 520 cm^{-1}. The accompanied volume change results in the appearance of the surface burs and the material dislodgements under grinding.

ACKNOWLEDGEMENT

The work was partially supported by the National Natural Science Foundation of China (NSFC) (Project No.: 51805257, 51475109 and 51275231).

REFERENCES

(1) H.Q. Sun, R. Irwan, H. Huang, G.W. Stachowiak, Surface characteristics and removal mechanism of cemented tungsten carbides in nanoscratching, Wear, 2010, **268**, p 1400-1408.

(2) B. Guo, Q. Zhao, M. Jackson, Precision grinding of binderless ultrafine tungsten carbide (WC) microstructured surfaces, Int. J. Adv. Manuf. Technol., 2013, **64**, p 727-735.

(3) P.G. Neudeck, L.G. Matus, An overview of silicon carbide device technology, AIP Conference Proceedings, 1992, **246**, p 246-253.

(4) Y. Lu, D. He, J. Zhu, X. Yang, First-principles study of pressure-induced phase transition in silicon carbide, Physica B, 2008, **403**, p 3543-3546.

(5) J. Ni, B. Li, Phase transformation in high-speed cylindrical grinding of SiC and its effects on residual stresses, Mater. Lett., 2012, **89**, p 150-152.

(6) N.R. Calderon, M. Martínez-Escandell, J. Narciso, F. Rodríguez-Reinoso, The combined effect of porosity and reactivity of the carbon preforms on the properties of SiC produced by reactive infiltration with liquid Si, Carbon, 2009, **47**, p 2200-2210.

(7) Q. Huang, L. Zhu, High-temperature strength and toughness behaviors for reaction-bonded SiC ceramics below 1400 °C, Mater. Lett., 2005, **59**, p 1732-1735.

(8) H. Liang, X. Yao, H. Zhang, X. Liu, Z. Huang, Friction and wear behavior of pressureless liquid phase sintered SiC ceramic, Mater. Des., 2015, **65**, p 370-376.

(9) J.N. Ness, T.F. Page, Microstructural evolution in reaction-bonded silicon carbide, J. Mater. Sci., 1986, **21**, p 1377-1397.

(10) J.J. Swab, A.A. Wereszczak, J. Pritchett, K. Johanns, Influence of microstructure on the indentation-induced damage in silicon carbide, Advances in Ceramic Armor II: Ceramic Engineering and Science Proceedings, 2007, **27**, p 251-259.

(11) B.R. Lawn, A.G. Evans, A model for crack initiation in elastic/plastic indentation fields, J. Mater. Sci., 1977, **12**, p 2195-2199.

(12) H.H.K. Xu, N.P. Padture, S. Jahanmir, Effect of microstructure on material-removal mechanisms and damage tolerance in abrasive machining of silicon carbide, J. Amer. Chem. Soc., 1995, **78**, p 2443-2448.

(13) S. Agarwal, P.V. Rao, Experimental investigation of surface/subsurface damage formation and material removal mechanisms in SiC grinding, Int. J. Mach. Tools Manuf., 2008, **48**, p 698-710.

(14) S. Agarwal, P.V. Rao, Grinding characteristics, material removal and damage formation mechanisms in high removal rate grinding of silicon carbide, Int. J. Mach. Tools Manuf., 2010, **50**, p 1077-1087.

(15) S. Agarwal, P. V. Rao, Improvement in productivity in SiC grinding, Proc. IMechE, Part B: J Engineering Manufacture, 2011, **225**, p 811-830.

(16) C. Li, F. Zhang, Z. Ma, Study on grinding surface deformation and subsurface damage mechanism of reaction-bonded SiC ceramics, Proc. IMechE, Part B: J Engineering Manufacture, 2016, p 1-10.

(17) F. Zhang, B. Meng, Y. Geng, Y. Zhang, Z. Li, Friction behavior in nanoscratching of reaction bonded silicon carbide ceramic with Berkovich and sphere indenters, Tribol. Int., 2016, **97**, p 21-30.

(18) C. Wu, B. Li, S.Y. Liang, A critical energy model for brittle–ductile transition in grinding considering wheel speed and chip thickness effects, Proc. IMechE, Part B: J Engineering Manufacture, 2016, **230**, p 1372-1380.

(19) B.V. Tanikella, A.H. Somasekhar, A.T. Sowers, R.J. Nemanich, R.O. Scattergood, Phase transformations during microcutting tests on silicon, Appl. Phys. Lett., 1996, **69**, p 2870-2872.

(20) A. Kailer, Y.G. Gogotsi, K.G. Nickel, Phase transformations of silicon caused by contact loading, J. Appl. Phys., 1997, **81**, p 3057-3063.

(21) H. Huang, J. Yan, New insights into phase transformations in single crystal silicon by controlled cyclic nanoindentation, Scr. Mater., 2015, **102**, p 35-38.

(22) Q. Zhang, S. To, Q. Zhao, B. Guo, G. Zhang, Impact of material microstructure and diamond grit wear on surface finish in micro-grinding of RB-SiC/Si and WC/Co carbides, Int. J. Refract. Met. Hard Mater., 2015, **51**, p 258-263.

(23) V. Domnich, Y. Gogotsi, S. Dub, Effect of phase transformations on the shape of the unloading curve in the nanoindentation of silicon, Appl. Phys. Lett., 2000, **76**, p 2214-2216.

(24) T.F. Page, W.C. Oliver, C.J. McHargue, The deformation behavior of ceramic crystals subjected to very low load (nano)indentations, J. Mater. Res., 1992, **7**, p 450-473.

(25) H. Huang, J.W. Yan, Possibility for rapid generation of high-pressure phases in single-crystal silicon by fast nanoindentation, Semicond. Sci. Technol., 2015, **30**, p 115001.

(26) L. Yin, H. Huang, Brittle materials in nano-abrasive fabrication of optical mirror-surfaces, Precis. Eng., 2008, **32,** p 336-341.

(27) J.B. Quinn, J. Yen, R.N. Katz, I.K. Lloyd, Subjective ceramic machinability and material properties, Mach. Sci. Technol., 2002, **6**, p 291-299.

(28) J.B. Quinn, G.D. Quinn, Indentation brittleness of ceramics: A fresh approach, J. Mater. Sci., 1997, **32**, p 4331-4346.

(29) B.R. Lawn, D.B. Marshall, Hardness, toughness, and brittleness: an indentation analysis, J. Amer. Chem. Soc., 1979, **62**, p 347-350.

(30) G.Z. Voyiadjis, R. Peters, Size effects in nanoindentation: an experimental and analytical study, Acta Mech., 2009, **211,** p 131-153.

(31) M.T. Laugier, New formula for indentation toughness in ceramics, J. Mater. Sci. Lett., 1987, **6**, p 355-356.

(32) S. Goel, X. Luo, P. Comley, R.L. Reuben, A. Cox, Brittle-ductile transition during diamond turning of single crystal silicon carbide, Int. J. Mach. Tools Manuf., 2013,

65, p 15-21.

(33) J. Gao, J. Chen, G. Liu, Y. Yan, X. Liu, Z. Huang, Role of microstructure on surface and subsurface damage of sintered silicon carbide during grinding and polishing, Wear, 2010, **270**, p 88-94.

(34) Y.Gogotsi, C. Baek, F. Kirscht, Raman microspectroscopy study of processing-induced phase transformations and residual stress in silicon, Semicond. Sci. Technol., 1999, **14**, p 936-944.

(35) T.G. Bifano, T.A. Dow, R.O. Scattergood, Ductile-regime grinding: a new technology for machining brittle materials, J. Manuf. Sci. Eng., 1991, **113**, p 184-189.

(36) Y.G. Gogotsi, V. Domnich, S.N. Dub, A. Kailer, K.G. Nickel, Cyclic nanoindentation and Raman microspectroscopy study of phase transformations in semiconductors, J. Mater. Res., 2000, **15**, p 871-879.